# Half-integer Mott-insulator phases in the imbalanced honeycomb lattice

Krzysztof Gawryluk,[1,2] Christian Miniatura,[1,3,4,5] and Benoît Grémaud[1,4,5,6]
[1]*Centre for Quantum Technologies, National University of Singapore, 3 Science Drive 2, Singapore 117543, Singapore*
[2]*Wydział Fizyki, Uniwersytet w Białymstoku, ulica Lipowa 41, 15-424 Białystok, Poland*
[3]*Institut Non Linéaire de Nice, UMR 7335, UNS, CNRS; 1361 route des Lucioles, 06560 Valbonne, France*
[4]*Merlion MajuLab, CNRS-UNS-NUS-NTU International Joint Research Unit UMI 3654, Singapore*
[5]*Department of Physics, National University of Singapore, 2 Science Drive 3, Singapore 117542, Singapore*
[6]*Laboratoire Kastler Brossel, Ecole Normale Supérieure CNRS, UPMC; 4 Place Jussieu, 75005 Paris, France*
(Received 27 February 2013; revised manuscript received 20 May 2014; published 20 June 2014)

Using mean-field theory, we investigate the ground-state properties of ultracold bosons loaded in a honeycomb lattice with on-site repulsive interactions and imbalanced nearest-neighbor hopping amplitudes. Taking into account correlations between strongly coupled neighboring sites through an improved Gutzwiller ansatz, we predict the existence of half-integer Mott-insulator phases, i.e., states with half-integer filling and vanishing compressibility. These insulating phases result from the interplay between quantum correlations and the topology of the honeycomb lattice, and could be easily addressed experimentally because they have clear signatures in momentum space.

DOI: 10.1103/PhysRevA.89.063615 PACS number(s): 67.85.Bc, 03.75.−b, 05.30.Rt, 67.85.Hj

## I. INTRODUCTION

Because of its remarkable low-energy electronic excitations, graphene has been the source of many key discoveries [1,2] which have sparked a vivid research flow now reaching new territories, as exemplified by ultracold atoms loaded in optical lattices [3–10]. In this paper, we address the bosonic Mott-insulator to superfluid (MI-SF) transition taking place in the honeycomb lattice [11,12] and show that the phase diagram is richer than for the square lattice [13–18]. Indeed, being genuinely bipartite, the honeycomb lattice has a two-site (labeled A and B) unit Bravais cell which can accommodate symmetric and antisymmetric states. This has dramatic consequences for the ground state of the interacting system, in either the Mott or superfluid phase. Strikingly, *half-integer* Mott lobes develop when nearest-neighbor hopping amplitudes are imbalanced. This situation is similar to the Kagome lattice [19–21], or more generally to any lattice for which the unit cell comprises more than one site, a situation which is unavoidable in the presence of an external magnetic field.

The paper is organized as follows. In Sec. II, we introduce the model and the extended Gutzwiller method [22–24] needed to correctly capture the intersite correlations responsible for these new half-integer Mott lobes. In Sec. III, we discuss the uncoupled dimer solutions, i.e., the properties of the Mott phases, at integer and half-integer fillings. In Sec. IV, we present our numerical results for the coupled dimers, in particular the transition from the Mott phase to the superfluid phase. In Sec. V, we discuss in more details the boundary of the half-filling Mott lobe properties, which can be obtained analytically emphasizing the transition from a quasi-one-dimensional (1D) situation to a two-dimensional (2D) square lattice phase diagram. The experimental signatures in momentum space, i.e., in the velocity distribution, of the different phases are discussed in Sec. VI. A summary of results and conclusions are given in Sec. VII.

## II. MODEL AND METHODS

Let us consider interacting bosons loaded on the honeycomb lattice with nearest-neighbor tunneling and further assume that one hopping parameter $J'$ is different from the two other (identical) ones $J$, see Fig. 1.

The limit $J' \ll J$ corresponds to weakly coupled 1D chains, whereas the limit $J' \gg J$ corresponds to weakly coupled dimers. It is worth noticing that hopping imbalance in the graphene lattice has already been achieved experimentally [6–10]. In the following we single out neighboring A and B sites coupled by $J'$, denote by $\mathbf{d}$ the vector joining them, and label by $\ell$ the $J'$ links they form. Note that $J'$ links form a rhombic lattice with coordination number $z = 4$. With this notation, the tight-binding Bose-Hubbard Hamiltonian [25] with on-site repulsive interactions reads

$$H = -J' \sum_{\ell} [a_\ell^\dagger b_\ell + b_\ell^\dagger a_\ell] - J \sum_{\langle \ell, \ell' \rangle} [a_\ell^\dagger b_{\ell'} + b_{\ell'}^\dagger a_\ell] + \frac{U}{2} \sum_{\ell} \left[ \hat{n}_a^\ell (\hat{n}_a^\ell - 1) + \hat{n}_b^\ell (\hat{n}_b^\ell - 1) \right] - \mu \sum_{\ell} \left[ \hat{n}_a^\ell + \hat{n}_b^\ell \right]. \quad (1)$$

Here $a_\ell^\dagger$ ($a_\ell$) and $b_\ell^\dagger$ ($b_\ell$) represent the creation (annihilation) operators associated with the endpoint sites A and B of the $J'$ link $\ell$. The corresponding number operators are $\hat{n}_a^\ell = a_\ell^\dagger a_\ell$ and $\hat{n}_b^\ell = b_\ell^\dagger b_\ell$. The (positive) interaction strength is $U$ and $\mu$ is the chemical potential. The summations run over all $J'$ links $\ell$ and, in the kinetic term, over their four nearest-neighbor $J'$ links $\ell'$ such that the A site on $\ell$ and the B site on $\ell'$ are nearest neighbors.

In the following, we investigate the zero-temperature phase diagram of Eq. (1) within a mean-field approach [22,23,26]. We mainly restrict our analysis to the dimer regime $J' > J$. As long as $J' < 2J$, the band structure of the noninteracting case ($U = 0$) depicts the celebrated conical intersections at the Dirac points around $E = 0$ and the system is a semimetal. At

 

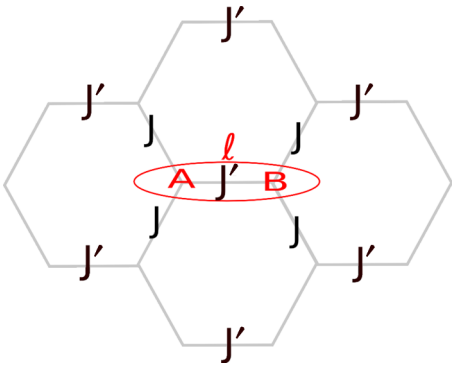


FIG. 1. (Color online) Honeycomb lattice geometry with imbalance hopping amplitudes $J'$ and $J$. When $J' \gg J$, the system can be described by weakly coupled A-B dimers living on the horizontal links denoted by $\ell$.

$J' = 2J$, the two Dirac points merge and the band structure undergoes a topological metal-insulator transition [3,4,27]. When $J' > 2J$, the band structure consists of two bands separated by $2(J' - 2J)$. When $J' \gg J$, this is simply the energy separation between the symmetric and antisymmetric dimer states $|\ell\pm\rangle = (|A\rangle_\ell \pm |B\rangle_\ell)/\sqrt{2}$ (energy $\mp J'$) built on each $J'$ link $\ell$. These dimer states give rise to the two preceding bands, each with a width $4J$ independent of $J'$. In this weak interlink coupling regime (or strong dimer regime), we expect the physics to be driven by the lower band and the MI-SF phase transition to be controlled by the ratio $J/U$. The Mott ground state is then well approximated by $\prod_\ell |n,\ell+\rangle$, $|n,\ell+\rangle$ being the Fock state with $n$ bosons in the symmetric state of link $\ell$. This state is beyond the reach of the standard Gutzwiller's ansatz which relies on a product of *on-site* states. This salient feature directly arises from the two-point topology of the graphene lattice and cannot happen with the square lattice where a strong imbalance of one hopping parameter leads to weakly coupled 1D chains. We improve Gutzwiller's ansatz by incorporating the correlations between $J'$ link sites and write the ground state as a product of *on link* states $|\text{g.s.}\rangle = \prod_\ell |\ell\rangle$:

$$|\ell\rangle = \sum_{n,m} f^{(\ell)}_{n,m} |n,A;m,B\rangle_\ell \quad \text{with} \quad \sum_{n,m} \left|f^{(\ell)}_{n,m}\right|^2 = 1, \tag{2}$$

$$= \sum_{p,q} g^{(\ell)}_{p,q} |p,+;q,-\rangle_\ell \quad \text{with} \quad \sum_{p,q} \left|g^{(\ell)}_{p,q}\right|^2 = 1, \tag{3}$$

where $|n,A;m,B\rangle_\ell$ is the Fock state on $J'$ link $\ell$ with $n$ atoms on site A and $m$ atoms on site B while $|p,+;q,-\rangle_\ell$ is the Fock state on the same $J'$ link $\ell$ with $p$ atoms in the symmetric state $|\ell+\rangle$ and $q$ atoms in the antisymmetric state $|\ell-\rangle$. Relating the $f^{(\ell)}_{n,m}$ and the $g^{(\ell)}_{p,q}$ is easy since the annihilation and creation operators for the $|\ell\pm\rangle$ states are $d^{(\dagger)}_{\ell,\pm} = (a^{(\dagger)}_\ell \pm b^{(\dagger)}_\ell)/\sqrt{2}$. If both Eqs. (2) and (3) represent the most general dimer state and fully describe the system on each $J'$ link, Eq. (3) proves more useful in the limit $J' \gg J$. The ground state of Eq. (1) has been obtained by imaginary-time evolution of an initial state with random values of amplitudes and periodic boundary conditions [13,28]. As the structure of the corresponding nonlinear time-dependent equations is rather involved, a 4th-order Runge-Kutta method was necessary.

## III. UNCOUPLED DIMERS

We first look for the ground state of the on-link dimer situation. It corresponds to the Mott states of Eq. (1). Figure 2 shows the on-site (left) and symmetric (right) average occupation numbers and their variances as functions of $\mu$ and $J'$ in units of $U$. When $J'/U$ is small, the on-site density depicts the usual Mott plateaus at integer fillings. But when $J'/U$ increases, one clearly observes the appearance of new plateaus at half-integer fillings. At the same time, plateaus at odd integer values $2p+1$ start to appear in the symmetric state density. For larger $J'/U$ values, each of these plateaus splits into two new ones with $2p+1$ and $2p+2$ fillings. Correspondingly (not shown here), the $|\ell-\rangle$-state occupation number decreases from the same value $2p+1$, at $J' = 0$, to an almost vanishing value. The plot of the on-site and symmetric variances emphasizes that the ground state of the system evolves from an on-site Fock state to an (almost) on-link Fock state when $J'/U$ increases. Indeed, when $J' \approx 0$, the on-site variance is almost zero while the $|\ell+\rangle$-state variance is the largest. Increasing $J'/U$, the on-site variance gets larger while the symmetric one almost vanishes. More precisely, the ground state is well approximated by Fock states $|n,A;n,B\rangle_\ell$ for $J' \approx 0$, whereas it is well approximated by Fock states $|p,+;0,-\rangle_\ell$ for larger $J'$.

Note that for $J'/U = 0.6$, the symmetric variance, albeit extremely small, is not strictly zero and even increases with $\mu$. The ground state is thus slightly contaminated by the $|\ell-\rangle$ states at finite $J'$ due to the interacting part of the Hamiltonian (1). Indeed only the latter is not diagonal in the $|\ell\pm\rangle$ basis and couples states $|p,+;q,-\rangle_\ell$ with the same total number of atoms $p+q$, $p$ and $q$ increments being by steps of 2. The actual ground state thus reads

$$|\text{g.s.}\rangle_1 = \alpha |\text{p},+;0,-\rangle_\ell + \sum_{\text{q}\leqslant\text{p}/2} \alpha_\text{q} |\text{p}-2\text{q},+;2\text{q},-\rangle_\ell. \tag{4}$$

In the large $J'/U$ limit, $\alpha$ is of the order of unity, whereas the other (small) coefficients are becoming smaller with increasing $q$ or $J'/U$. Except for $p = 0$ and $p = 1$, $n^\ell_+$ is always a bit less than an integer and the symmetric variance is never strictly zero, even if discrepancies go to 0 when increasing $J'/U$. This is clearly seen in Fig. 2(f) at $J'/U = 0.6$ (dot-dashed line) where the variance deviates from zero only for plateaus with symmetric filling $p \geqslant 2$ (solid line). For small $J'/U$ values, the ground state simply becomes $|n,A;n,B\rangle_\ell$, such that the coefficients $\alpha_q$ are now given by $(-1)^q/(n-q)!q!$ (up to a normalization factor). They reach a maximum for $q = n/2$, leading to the same number of bosons in the $|\ell\pm\rangle$ states. This corresponds to an even-integer symmetric filling $p = 2n$ in Eq. (4). For odd filling $p = 2n+1$, Eq. (4) is not the ground state of the system when $J' = 0$. However, increasing $J'$ lowers the energy of the $|\ell+\rangle$ state, which compensates for the additional energy cost for this extra boson. State Eq. (4) with $2n+1$ bosons then becomes more favorable in a given range of $\mu/U$. The actual scenario is of course less simple since at intermediate values of $J'/U$, the ground state does not correspond to a pure Fock state in any

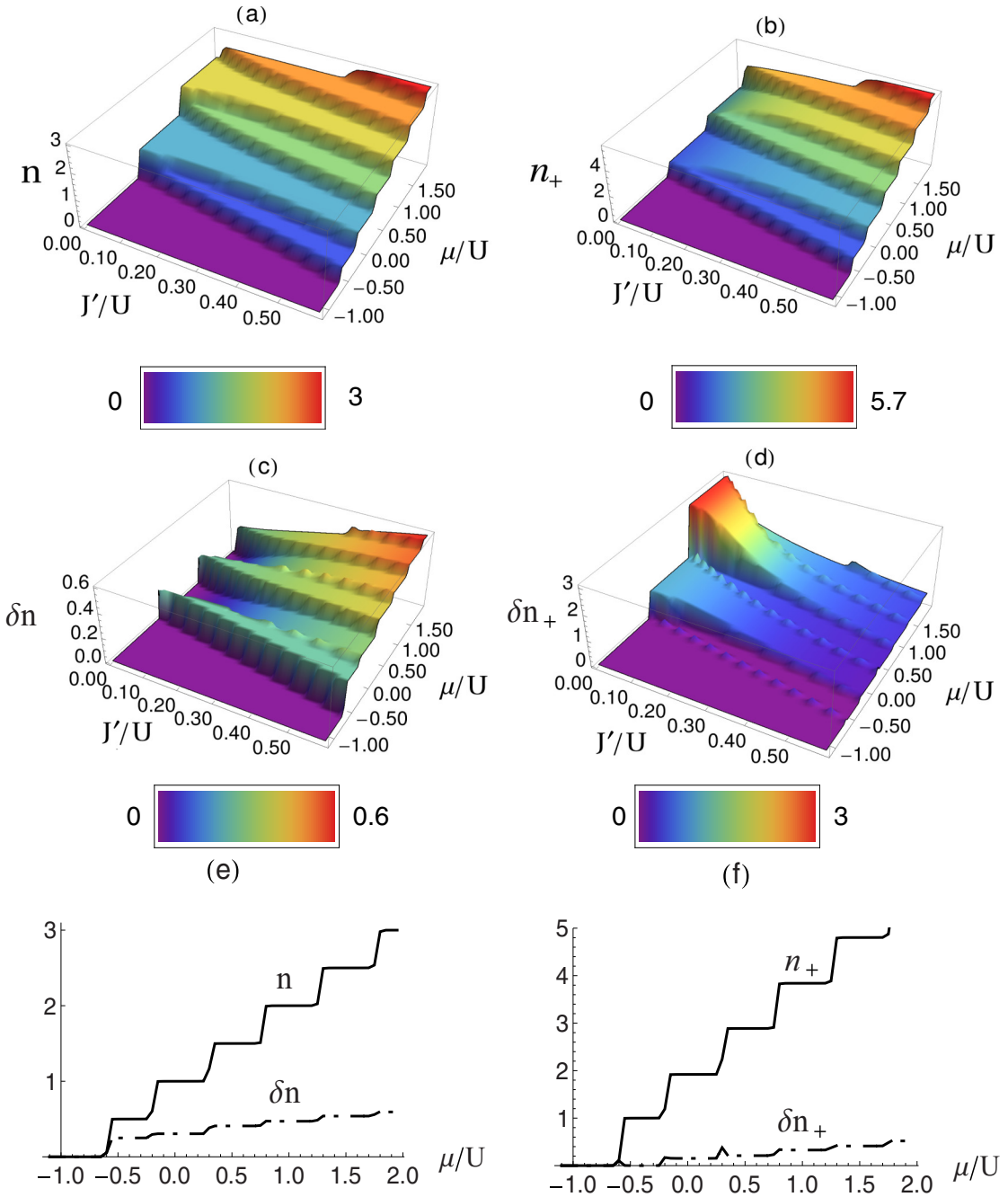


FIG. 2. (Color online) Phase diagram of Hubbard Hamiltonian (1) for $J = 0$. Left: on-site density $n$ (a) and variance $\delta n$ (c) as a function of $J'/U$ and $\mu/U$ with their color codes. Plot (e) is a cut of (a) and (c) for $J'/U = 0.6$. Right: same as left but for the symmetric density $n_+$ and variance $\delta n_+$. For large $J'/U$, the on-site density depicts plateaus at half-integer fillings, corresponding to integer occupation numbers of the symmetric states $|\ell+\rangle$. The bottom plots emphasize that the first plateau corresponds to the Fock state $|1,+;0,-\rangle_\ell$.

of the two bases. For instance, the Mott state at unit filling reads

$$\begin{aligned}|M1\rangle &= c|2,+;0,-\rangle - s|0,+;2-\rangle \\ &= \frac{c-s}{2}(|2,A;0,B\rangle + |0,A;2,B\rangle) \\ &\quad + \frac{c+s}{\sqrt{2}}|1,A;1,B\rangle,\end{aligned}$$

$$\text{with} \quad c^2 = \frac{1}{2}\left[1 + \frac{4J'}{\sqrt{(4J')^2+U^2}}\right], \quad s^2 = \frac{1}{2}\left[1 - \frac{4J'}{\sqrt{(4J')^2+U^2}}\right]. \tag{5}$$

In the limit $J' \ll U$, one recovers the usual Mott state $|1,A;1,B\rangle$, whereas in the limit $J' \gg U$, as explained above, the Mott state is simply the symmetric state $|2,+;0,-\rangle$. Whereas the onsite density is independent of $J'/U$, the

difference between the symmetric and antisymmetric occupation numbers is $2(c^2 - s^2) = 8J'/\sqrt{(4J')^2 + U^2}$, ranging from 0 for $J' \ll U$ to 2 for $J' \gg U$. As explained in Sec. VI, this feature can be inferred from the velocity distribution of the atoms.

## IV. COUPLED DIMERS

We now consider the $(J'/U, \mu/U)$ phase diagram obtained in the $|\ell+\rangle$ states when $J$ is nonzero. As seen in Figs. 3(a) and 3(b), the situation is very much similar to the usual MI-SF transition. One finds regions with constant symmetric occupation numbers $n_+$ and almost vanishing variance, corresponding to a Mott state with vanishing compressibility $\chi = \partial n/\partial\mu$. These Mott lobes are surrounded by a superfluid sea where $\chi$ is finite. For small $J/U$, the lower Mott plateaus are still well visible, whereas the higher plateaus are almost all smoothed out; see Fig. 3(c) where the variance of the first two Mott phases is still small. Between the plateaus, the variance has maxima revealing the superfluid phases. For $\mu \gtrsim U$, $n_+$ varies smoothly and the system is superfluid. For larger values of $J/U$, the half-integer Mott lobes almost entirely disappear except at very low values of $J'/U$, see Fig. 3(b). This is further exemplified by Fig. 3(d) where both $n_+$ and $\delta n_+$ vary smoothly as $\mu$ is increased. The evolution of the $g^{(\ell)}_{p,q}$ amplitudes when $J$ increases at fixed $J'$ is similar to the MI-SF scenario in the usual Gutzwiller's ansatz. When $J'/U$ is large, $g^{(\ell)}_{p,q} = \delta_{pp_0}\delta_{q0}$ and the Mott state is approximated by the Fock state $|p_0,+;0,-\rangle_\ell$. At the transition, the distribution $g^{(\ell)}_{p,q}$ starts broadening, but only in the *symmetric* direction $q = 0$ and the physics takes place entirely in the symmetric subspace. For instance, when $J' \gg J \gg U$, the superfluid phase at density $\rho$ is described by the coherent state $|\sqrt{\rho}\rangle_+ \otimes |0\rangle_-$ with no bosons in the antisymmetric subspace. For intermediate $J'/U$, the Mott state is slightly contaminated by antisymmetric contributions. The MI-SF transition scenario remains, however, the same: the $g^{(\ell)}_{p,q}$ still spread along the symmetric direction and keep a structure similar to Eq. (4).

The phase diagrams in the $(J/U, \mu/U)$ plane are shown in Figs. 4–6 for three different values of $J'$, namely, $J'/U = 0.1$, $J'/U = 0.5$, and $J'/U = 1$. As expected, the size of the half-integer Mott plateau increases with increasing $J'$, whereas the size of the integer ones is decreasing. More precisely, in the large $J'/U$ limit, the different Mott states are simply $|p,+;0-\rangle$, with a free energy given by $E^+_p = Up(p-1)/4 - (J'+\mu)p$. Therefore, along the $J = 0$ axis, the transition between the $p$ and $p+1$ Mott phases occurs for $\mu = -J' + pU/2$, such that all Mott states have the same width $U/2$. For an arbitrary value of $J'$, the transition, along the $J = 0$ axis, between the different Mott phases is more complicated to determine due to the nontrivial structure of the Mott states, see Eq. (4). Nevertheless, in the case of the half-integer Mott phase, one can simply obtain the $J = 0$ boundary:

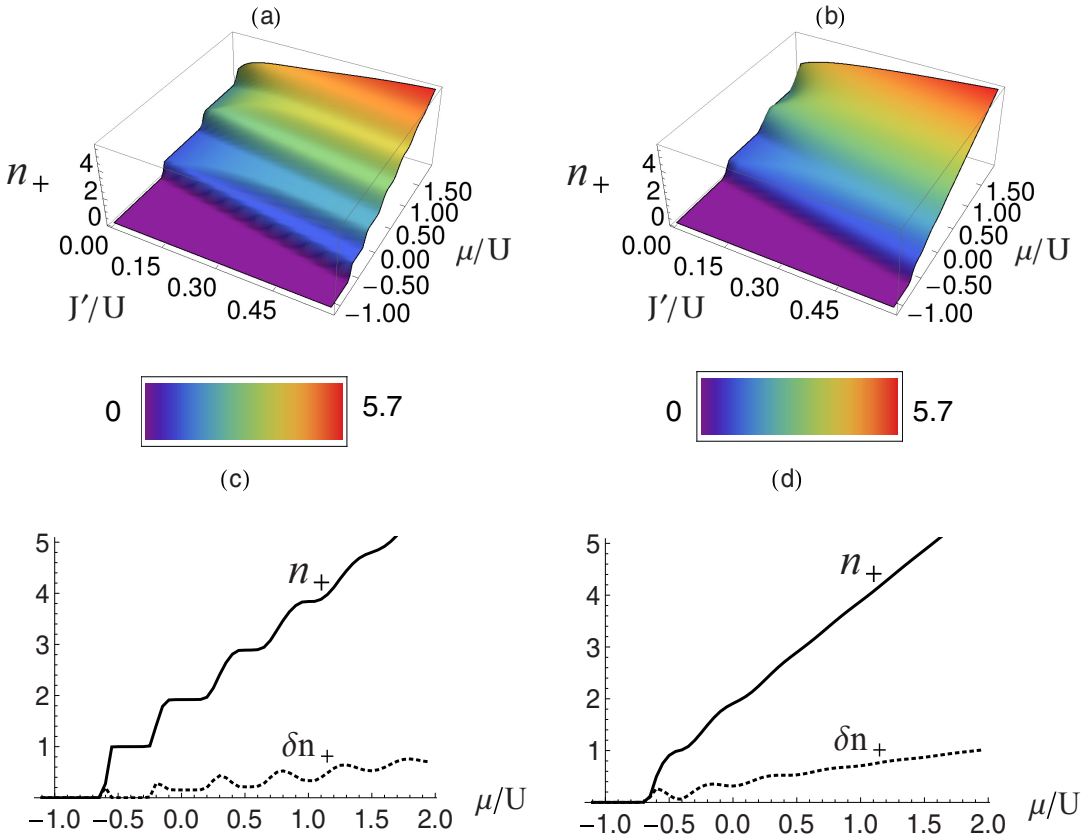


FIG. 3. (Color online) Phase diagram of Hubbard Hamiltonian (1). Left column: $J/U = 0.015$. Right column: $J/U = 0.04$. (a), (b): occupation number $n_+$ as a function of $J'/U$ and $\mu/U$ with the color code. (c), (d): $n_+$ and $\delta n_+$ as a function of $\mu/U$ for $J'/U = 0.6$. For $J/U = 0.015$, the first three Mott plateaus are clearly visible, whereas they are smoothed out for $J/U = 0.04$.

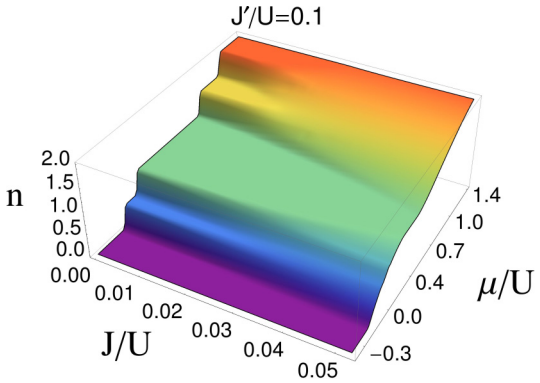


FIG. 4. (Color online) Phase diagram in the $(J/U,\mu/U)$ plane for a fixed value of $J'/U = 0.1$. For this small value of $J'$, the dominant Mott phases correspond to integer fillings, whereas the half-integer Mott phase depicts a much smaller extension. For instance, the $n = 0.5$ Mott lobe corresponds to $-J' < \mu < J'$, for $J = 0$, whereas the tip of the lobe corresponds to $J \approx J'/4$.

$-J' < \mu < J' + U/2 - \sqrt{U^2 + (4J')^2}/2$. In particular, in the limit $J' \ll U$, one obtains $-J' < \mu < J'$, in agreement with Fig. 4. In addition, one can see that the half-integer Mott lobe always corresponds to $J$ values much lower than $J'$, i.e., the situation of weakly coupled dimers.

The preceding analysis shows that the half-integer Mott lobes are observed in the regime $J \ll J' \lesssim U$ and that for a fixed value of $J'$, the Mott-superfluid transition occurs for values of the parameter $J/U \approx 10^{-2}$, similar to the usual Mott-superfluid transition. In addition, deep inside the Mott phase, the gap is expected to be of the order of $J'$ or larger. Therefore, for temperatures such that $k_B T \ll J$, its impact on the system properties is expected to be comparable to the standard situation, and thus the half-integer Mott lobes are within experimental reach. A full description of these finite temperature effects can be obtained from the mean-field excitations spectrum, i.e., the Bogoliubov modes, but this is beyond the scope of the paper.

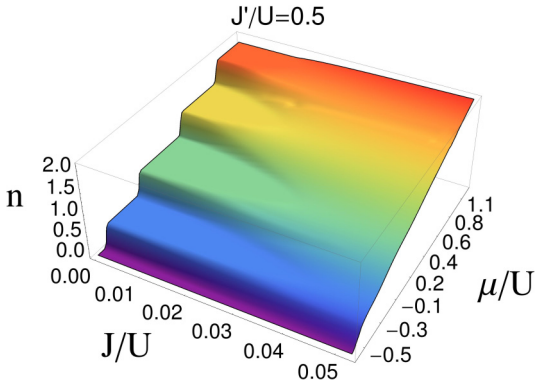


FIG. 5. (Color online) Phase diagram in the $(J/U,\mu/U)$ plane for a fixed value of $J'/U = 0.5$. The half-integer Mott phases have a larger extension, but still smaller than the integer ones.

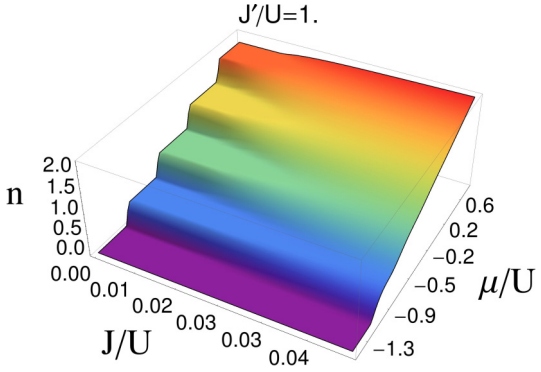


FIG. 6. (Color online) Phase diagram in the $(J/U,\mu/U)$ plane for a fixed value of $J'/U = 1$. As explained in the text, the situation corresponds to weakly coupled dimers, such that the phase diagram resembles the one of the square lattice: all Mott lobes have the same width $U$ (for $J = 0$), the transition from the Mott phase with $p$ bosons in the symmetric state, corresponding to a lattice filling $p/2$, to the Mott phases with $p + 1$ bosons occurs for $\mu = -J' + pU/2$. The tip of the Mott lobe with $p$ bosons in the symmetric state is given by $U/J_{c4}^{(p)} = 4[2p + 1 + 2\sqrt{p(p+1)}]$.

## V. CRITICAL HOPPING AMPLITUDE

We obtain the MI-SF critical hopping rate $J_c$ by monitoring the tip of the two first Mott lobes, see Fig. 7. For integer filling, the usual Bose-Hubbard model predicts $U/J_{cz}^{(\rho)} = z[2\rho + 1 + 2\sqrt{\rho(\rho+1)}]$, where the average density $\rho$ is here an integer and $z$ is the lattice coordination number [22,23]. For small $J'/U$, we have $z = 2$ (almost independent 1D chains) and the physics is driven by on-site Fock states, the main Mott lobe being at $\rho = n = 1$. For imbalanced hopping parameters, one gets $(2J + J') = U/5.8$ and thus $J_c = J_{c2}^{(1)} - J'/2$. This prediction correctly reproduces our numerical results at small $J'/U$. In the large $J'/J$ limit, however, the physics takes place in the symmetric subspace and $z = 4$ (dimer lattice). It is easy to see from Eq. (1) that the effective hopping parameter in the dimer lattice is $J/2$ giving rise to a noninteracting band with finite width $4J$ independent of $J'$, such that in the large $J'/U$ limit, $J_c$ for the Mott lobe at $\rho = n_+ = 1$ (equivalently $n = 0.5$) reaches the value $J_{c4}^{(1)}$. In addition, for large $J'/U$, $J_c$ for the Mott lobe at $n = 1$ ($n_+ = 2$) saturates, as it should, at $J_{c4}^{(2)}$ ($z = 4$, $\rho = n_+ = 2$).

As explained above, the half-integer Mott state is simply $|1,+;0-\rangle$, such that the boundary between the Mott and the superfluid phase can be obtained analytically. More precisely, close to the boundary, a first-order perturbation theory leads to the following expression for the ground state (on a given link $\ell$):

$$|\psi\rangle = |1,+;0-\rangle + \sum_k |k\rangle \frac{\langle k|V|1,+;0-\rangle}{E_{10} - E_k}, \qquad (6)$$

where $|k\rangle$ are the different states coupled to $|1,+;0-\rangle$ by the mean-field kinetic energy term

$$V = -2J(\langle d_+\rangle d_+^\dagger + \langle d_+^\dagger\rangle d_+ - \langle d_-\rangle d_-^\dagger - \langle d_-^\dagger\rangle d_-). \qquad (7)$$

The states coupled by $V$ are therefore $|1,+;1-\rangle$, $|2,+;0-\rangle$ and $|0,+;0-\rangle$, but the states $|k\rangle$ in Eq. (6) must be eigenstates

of the on-link Hamiltonian, such that the relevant states are

$$\begin{aligned} &|0,+;0-\rangle, \quad |1,+;1-\rangle, \\ &|+\rangle = c|2,+;0-\rangle - s|0,+;2-\rangle, \\ &|-\rangle = s|2,+;0-\rangle + c|0,+;2-\rangle, \end{aligned} \tag{8}$$

where $c$ and $s$ are defined in Eq. (5). $|+\rangle$ is nothing but the $n = 1$ Mott state, an eigenstate of the on-link Hamiltonian. The notation $\langle d_\pm \rangle$ corresponds to the ground-state average value $\lambda_\pm = \langle \psi | d_\pm | \psi \rangle$, which must be self-consistently obtained using the ground-state expression given by Eq. (6) [14,23]. $\lambda_\pm$ are precisely the mean-field order parameters, with vanishing values in the Mott state, and nonzero values in the superfluid phase. From the first-order perturbation expression (6), one obtains that the boundary between the two phases is given by the following equation:

$$\frac{1}{4J} = \frac{1}{2}\frac{1}{J'+\mu} + \frac{c^2}{J'-\mu+E_-} + \frac{s^2}{J'-\mu+E_+}, \tag{9}$$

where $E_\pm$ are the energies of the states $|\pm\rangle$, namely, $E_\pm = \frac{U}{2} \pm \frac{1}{2}\sqrt{U^2+(4J')^2}$. For $J \to 0$, the boundary corresponds to either $\mu = -J'$ or $\mu = J' + E-$, which are exactly the two values given in the preceding section (since $E_+ > E_-$, the boundary is given by the $E_-$ term). The critical value of $J_c$, i.e., the tip of the Mott lobe, is the largest $J$ value on the boundary and is thus given by the minimum value of the right-hand side of Eq. (9), for $-J' < \mu < J' + E_-$. In the small $J'/U$ limit, the critical value $J_c$ for the half-integer Mott phase scales like $J'/4$, a value within experimental reach, see Ref. [10] where $J'/J = 10$ has been achieved. In the large $J'/U$ limit, one obtains that $J_c = J_{c4}^{(1)}(1 - \frac{1}{8}\frac{U}{J'})$, in good agreement with our numerical data for $\rho = n_+ = 1$ (equivalently $n = 0.5$), see the blue dashed line in Fig. 7. In principle, the boundary between the superfluid and the Mott phase for higher fillings could be obtained in a similar way, the final expressions are quite involved, and therefore not put in this paper.

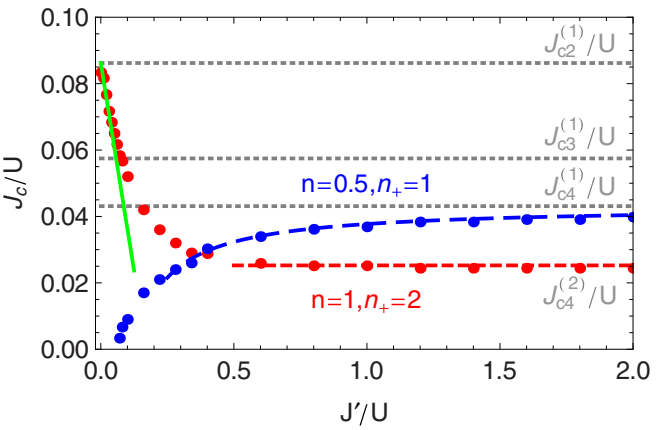


FIG. 7. (Color online) Critical hopping $J_c$ for the MI-SF transition as a function of $J'$ (in units of $U$). Red (blue) dots are numerical data obtained with the extended Gutzwiller's ansatz for the $n = 1$ ($n = 0.5$) Mott lobe. Continuous and long-dashed lines are analytical predictions. The horizontal black dashed lines correspond to the critical values $J_{cz}^{(1)}$ ($z = 1,2,3$). See text for details.

Finally, even though the present ansatz favors $J'$ links over $J$ links, it is quite remarkable that our numerical results for the Mott lobe at $\rho = n = 1$ cross the critical value $J_{c3}^{(1)}$ of the balanced honeycomb lattice roughly when $J_c = J'$. From that point of view, the system undergoes a crossover from a quasi-1D situation with two neighbors (weakly coupled chains) to a 2D situation with four neighbors, the balanced honeycomb lattice with three neighbors being the intermediate situation.

## VI. EXPERIMENTAL SIGNATURES

The momentum distribution of the atoms, measured after the optical lattice is rapidly switched off, is known to exhibit a clear signature of the MI-SF transition [15,29]. One can show that

$$n_{\mathbf{k}} \propto \sum_{i,j} \langle \text{g.s.}|c_i^\dagger c_j|\text{g.s.}\rangle \exp\left[i\mathbf{k}\cdot(\mathbf{R}_j - \mathbf{R}_i)\right], \tag{10}$$

where $\mathbf{R}_i$ is the position of site $i$. Since the usual Gutzwiller's ansatz discards intersite correlations, only terms like $\langle c_i^\dagger c_i \rangle$ or $\langle c_i^\dagger \rangle \langle c_j \rangle \exp[i\mathbf{k}\cdot(\mathbf{R}_j - \mathbf{R}_i)]$ contribute to $n_{\mathbf{k}}$. Our extended ansatz includes the additional terms $\langle a_\ell^\dagger b_\ell \rangle \exp(i\mathbf{k}\cdot\mathbf{d})$ which give rise to a periodic modulation of the velocity distribution,

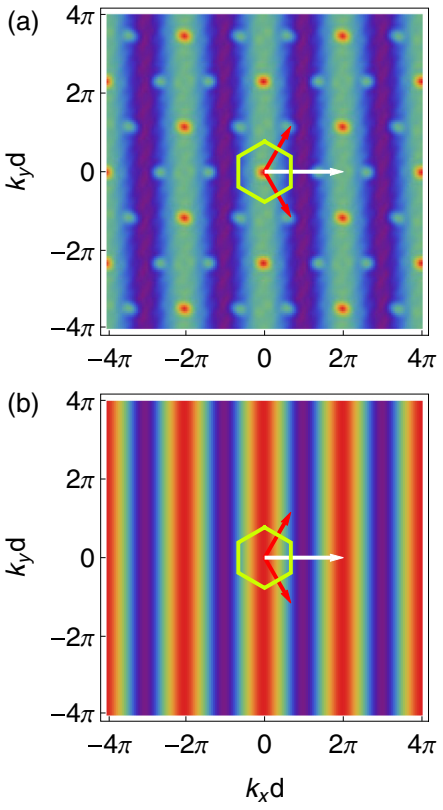


FIG. 8. (Color online) Momentum distribution $n_{\mathbf{k}}$ for $J/U = 0.015$, $J'/U = 0.6$. (a) SF phase ($\mu/U = -0.14$). (b) MI phase ($\mu/U = -0.5$). The hexagon is the first Brillouin zone with its reciprocal lattice vectors (red dark arrows). The $J'$ link $\mathbf{d}$ vector is chosen along $Ox$. The periodic stripes (with period $2\pi/d$ shown by the white arrow) are a signature of the quantum correlations between the A and B sites along $J'$ links. See text for details.

a smoking-gun of a Mott phase built on a symmetric state. For a pure Fock state $|p,+;0,-\rangle$, $n_{\mathrm{MI}}(\mathbf{k}) = p[1+\cos(\mathbf{k}\cdot\mathbf{d})]$ and the modulation contrast is $C = 1$. With the actual ground state of Eq. (4), $C \leqslant 1$. In general, measuring the contrast $C$ for Mott states with $n \geqslant 1$ would reveal that they are not simple Fock states with fixed on-site density but have an underlying structure. For instance, $C = J'/\sqrt{J'^2 + (U/4)^2}$ for the Mott state $n = 1$. For the superfluid state, a product of on-site coherent states, one finds $n_{\mathrm{SF}}(\mathbf{k}) = \rho_0 \sum_{ij} e^{i\mathbf{k}\cdot(\mathbf{R}_j - \mathbf{R}_i)}$ (assuming a uniform density $\rho_0$), which depicts peaks at the reciprocal lattice vectors modulated by the square of the structure factor of the lattice. The additional on-link correlations thus show up as an additional modulation on top of this ideal distribution. All these properties are confirmed by our numerical calculations, see Fig. 8, where both the superfluid [Fig. 8(a)] and the Mott [Fig. 8(b)] phases display a periodic modulation along $\mathbf{d}$ with period $2\pi/d$ ($d = |\mathbf{d}|$). Note that besides the preceding modulation, the effect of the structure factor in the superfluid phase is clearly visible in the different peak heights.

## VII. CONCLUSION

In conclusion, using an extended Gutzwiller's ansatz, we have described the properties of the MI-SF transition of ultracold bosons in a honeycomb lattice. We have found Mott phases at *half-integer* fillings, arising directly from the interplay between quantum correlations and the topology of the honeycomb lattice. Future work will address the excitations of the system [30] as they can lead to additional experimental signatures. Finally, it would be interesting to study the impact of an external (non-Abelian) gauge field on the properties of the ground state [31–33].

## ACKNOWLEDGMENTS

The Centre for Quantum Technologies is a Research Centre of Excellence funded by the Ministry of Education and National Research Foundation of Singapore. Ch.M. is a Fellow of the Institute of Advanced Studies (NTU).

[1] K. S. Novoselov *et al.*, Science **306**, 666 (2004).
[2] A. H. Castro Neto *et al.*, Rev. Mod. Phys. **81**, 109 (2009).
[3] S.-L. Zhu, B. Wang, and L.-M. Duan, Phys. Rev. Lett. **98**, 260402 (2007).
[4] K. L. Lee, B. Grémaud, R. Han, B.-G. Englert, and C. Miniatura, Phys. Rev. A **80**, 043411 (2009).
[5] Z. Y. Meng, T. C. Lang, S. Wessel, F. F. Assaad, and A. Muramatsu, Nature **464**, 847 (2010).
[6] P. Soltan-Panahi *et al.*, Nat. Phys. **7**, 434 (2011).
[7] P. Soltan-Panahi *et al.*, Nat. Phys. **8**, 71 (2012).
[8] L. Tarruell, D. Greif, T. Uehlinger, G. Jotzu, and T. Esslinger, Nature **483**, 302 (2012).
[9] T. Uehlinger, G. Jotzu, M. Messer, D. Greif, W. Hofstetter, U. Bissbort, and T. Esslinger, Phys. Rev. Lett. **111**, 185307 (2013).
[10] D. Greif, T. Uehlinger, G. Jotzu, L. Tarruell, and T. Esslinger, Science **340**, 1307 (2013).
[11] I. Kimchi, S. A. Parameswaran, A. M. Turner, and A. Vishwanath, Proc. Natl. Acad. Sci. USA **110**, 16378 (2013).
[12] Zhu Chen and Biao Wu, Phys. Rev. Lett. **107**, 065301 (2011).
[13] S. Sachdev, *Quantum Phase Transitions* (Cambridge University, Cambridge, England, 2001).
[14] D. Jaksch, C. Bruder, J. I. Cirac, C. W. Gardiner, and P. Zoller, Phys. Rev. Lett. **81**, 3108 (1998).
[15] M. Greiner, O. Mandel, T. Esslinger, T. W. Hänsch, and I. Bloch, Nature **415**, 39 (2002).
[16] I. B. Spielman, W. D. Phillips, and J. V. Porto, Phys. Rev. Lett. **98**, 080404 (2007).
[17] I. B. Spielman, W. D. Phillips, and J. V. Porto, Phys. Rev. Lett. **100**, 120402 (2008).
[18] M. Rigol, G. G. Batrouni, V. G. Rousseau, and R. T. Scalettar, Phys. Rev. A **79**, 053605 (2009).
[19] L. Santos, M. A. Baranov, J. I. Cirac, H.-U. Everts, H. Fehrmann, and M. Lewenstein, Phys. Rev. Lett. **93**, 030601 (2004).
[20] B. Damski, H. Fehrmann, H.-U. Everts, M. Baranov, L. Santos, and M. Lewenstein, Phys. Rev. A **72**, 053612 (2005).
[21] S. A. Parameswaran, Itamar Kimchi, Ari M. Turner, D. M. Stamper-Kurn, and Ashvin Vishwanath, Phys. Rev. Lett. **110**, 125301 (2013).
[22] W. Zwerger, J. Opt. B: Quantum Semiclass. Opt. **5**, S9 (2003).
[23] A. Georges, in *Ultracold Fermi Gases, Proceedings of the International School of Physics Enrico Fermi, Varenna, 20–30 June 2006, Course CLXIV*, edited by M. Inguscio, W. Ketterle, and C. Salomon (IOS Press, Amsterdam, 2007), p. 477.
[24] C. Trefzger, C. Menotti, B. Capogrosso-Sansone, and M. Lewenstein, J. Phys. B: At. Mol. Opt. Phys. **44**, 193001 (2011).
[25] M. P. A. Fisher, P. B. Weichman, G. Grinstein, and D. S. Fisher, Phys. Rev. B **40**, 546 (1989).
[26] W. Ketterle, D. S. Durfee, and D. Stamper-Kurn, in *Bose-Einstein Condensation in Atomic Gases, Proceedings of the International School of Physics Enrico Fermi, Varenna, 7–17 July 1998, Course CXL*, edited by M. Inguscio, S. Stringari, and C. Wieman (IOS Press, Amsterdam, 1999), p. 67.
[27] G. Montambaux, F. Piéchon, J.-N. Fuchs, and M. O. Goerbig, Phys. Rev. B **80**, 153412 (2009).
[28] M. Lewenstein *et al.*, Adv. Phys. **56**, 243 (2007).
[29] I. Bloch, J. Dalibard, and W. Zwerger, Rev. Mod. Phys. **80**, 885 (2008).
[30] T. Stöferle, H. Moritz, C. Schori, M. Köhl, and T. Esslinger, Phys. Rev. Lett. **92**, 130403 (2004).
[31] A. Górecka, B. Grémaud, and C. Miniatura, Phys. Rev. A **84**, 023604 (2011).
[32] J. Dalibard, F. Gerbier, G. Juzeliūnas, and P. Öhberg, Rev. Mod. Phys. **83**, 1523 (2011).
[33] A. Bermudez *et al.*, New J. Phys. **12**, 033041 (2010).